Pergamon

PII: S1359-6454(98)00231-6

Acta mater. Vol. 46, No. 16, pp. 5611–5626, 1998

Published by Elsevier Science Ltd.

Printed in Great Britain
1359-6454

OVERVIEW NO. 130

SIZE EFFECTS IN MATERIALS DUE TO MICROSTRUCTURAL AND DIMENSIONAL CONSTRAINTS: A COMPARATIVE REVIEW

E. ARZT

Max-Planck-Institut für Metallforschung and Institut für Metallkunde der Universität, Seestr. 92, D-70174 Stuttgart, Germany

(Received 4 May 1998; accepted 9 June 1998)

Abstract—Effects of size on predominantly mechanical properties of materials are reviewed at a first-order level. Microstructural constraints, e.g. due to second-phase particles and grain boundaries, and dimensional constraints in small-scale materials such as thin films are distinguished. Phenomena addressed are particle strengthening in plasticity, creep and magnetism, grain size strengthening and the limits to Hall–Petch behavior as well as the yielding of thin films and multilayers. Important aspects can be understood from the point-of-view of the interaction of a characteristic length (which may be as diverse as the dislocation radius of curvature at a given stress or the magnetic exchange length) with a size parameter (grain or particle size, or film thickness). It is demonstrated that such an approach can reveal interesting analogies between otherwise very different properties of materials.

1. INTRODUCTION

The science of materials is, to a large extent, couched in terms of length scales and their interactions. Its domain ranges from the behavior of individual atoms to macroscopic aspects of materials properties. What distinguishes classical materials science from its neighboring disciplines of, e.g. solid state physics and chemistry, on the one hand, and from materials technology and mechanical design, on the other, is its preoccupation with the intermediate level between the atomistic and the macroscopic range—that of *microstructure*. For the sake of definition, microstructure is usually meant to encompass the arrangement of crystallites (of equal or differing phase constitution) and of the crystal defects (excluding those which are present in thermal equilibrium, such as vacancies).

The microstructure of a material is controlled by the processing steps chosen for its fabrication. Such microstructural design affects the nature of the phases present, their topology (i.e. geometrical distribution and interconnection) and their dispersion (described by relevant "size" parameters). The full characterization of these parameters is the domain of quantitative metallurgy (e.g. Ref. [1]). Some of the quantities which will be dealt with in the present paper are illustrated in Fig. 1, and the symbols used throughout the text are compiled in Appendix A.

All other parameters of the microstructure being equal, its size parameters exert a strong influence on the materials properties. In fact, it is this variability of the property spectrum through microstructural control that has often led to new materials of metallic, but also of ceramic and of polymeric origin. Most of these size effects come about because of the *microstructural constraint* to which a particular physical mechanism is subjected. Consider the classic case of strengthening a metallic matrix by particles or grain boundaries: lattice dislocations are forced, by the microstructural constraint, to bow out or pile up, which requires an external stress characteristic of a microstructural parameter. An analogous case is the "magnetic strength" of a ferromagnet, which reflects the ease of motion of magnetic domain walls; here, the wall thickness relative to the size of the microstructural inhomogeneity can control the macroscopic behavior.

In general, it is therefore the competition or coupling between two different size dependencies that determines the properties of a material. We thus have to deal with the interaction of two length scales: one is the dimension characteristic of the physical phenomenon involved, called the *characteristic length* throughout this paper. The other is some microstructural dimension, denoted as the *size parameter*. The range in which these two quantities overlap is of particular interest: here conventional size laws often break down and may even be reversed.

Apart from microstructural constraints, a new element relevant for this paper has been introduced in recent years by the developments in micro-tech-

Fig. 1. Microstructural constraints: examples of size parameters include grain size D, grain boundary width δ_b, obstacle spacing L, and obstacle radius R; characteristic lengths, which are connected with a physical mechanism, can be the equilibrium diameter d of a dislocation loop, the spacing w between partial dislocations, or the width δ of a magnetic domain wall. Special macroscopic behavior results when the ranges of characteristic lengths and of size parameters overlap.

nology: the fabrication of thin films, multilayers and micro-machined components used in microelectronic and micromechanical systems requires materials to be tailored to small component dimensions. In these cases, the physical mechanism may begin to "feel" the presence of the surface or an interface; as a result, a *dimensional constraint* can appear which superimposes on that of the microstructure (Fig. 2). With ever-continuing miniaturization, an understanding of these effects will be of increasing relevance, both for fundamental reasons and in the interest of the reliability of small-scale systems. Compared to electronic size effects, which arise from the constraint of electron waves in small structures, the interactions of defects with geometrical constraints are less well understood and merit further attention.

The purpose of this paper is to provide a synopsis of such size effects, both through microstructural and dimensional constraints, on materials properties. On closer inspection it becomes apparent that materials science abounds with size effects, many of which cannot be included in the present text. The selection favors mechanical phenomena in predominantly metallic materials, and parallels are drawn to magnetic properties. The central theme will be the interaction of microstructure or film dimensions, on the one hand, with the characteristic length, on the

Fig. 2. Dimensional constraints: when the external dimensions of components become small, they can control the material behavior. An example is a thin film, in which the film thickness H is the relevant size parameter. This parameter can interact with microstructural parameters (such as grain size D, particle spacing L, etc.) and with characteristic lengths as in Fig. 1.

other. The approach, being rather tutorial, gives simple formulations of first-order effects; for more sophisticated treatments the reader will be referred to the literature.

2. MECHANICAL STRENGTHENING OF METALS BY MICROSTRUCTURAL CONSTRAINTS

Strengthening of pure metals can be achieved by solute atoms (“solid solution hardening”), by cold deformation (“work hardening”), by precipitates or hard dispersoids (“precipitation”, or “dispersion strengthening”) or by grain size refinement. Through these technologically important alloying strategies, the hardness of metallic alloys can be varied over more than two orders of magnitude. In all cases, the strengthening effect is due to obstacles which block or retard the motion of lattice dislocations. These processes are prime examples of size effects due to length scale interaction.

The most fundamental “characteristic length” of a lattice dislocation is the magnitude b of its Burgers vector, which characterizes the strength of the lattice distortion caused by its presence. The resulting “line tension” imparts to the dislocation a resistance against bending. A related characteristic length is therefore the equilibrium diameter a curved dislocation (or a dislocation loop) assumes under a shear stress τ. Assuming elastic isotropy, this diameter is given by

$$d(\tau) = \frac{2T_d}{b\tau} \approx \frac{Gb}{\tau} \tag{1}$$

where $T_d \approx Gb^2/2$ is a simplified expression for the line tension and G is the shear modulus of the matrix material. The relevant size parameter against which this diameter must be compared depends on the nature of the obstacle, as will now be discussed.

2.1. Particle strengthening in plasticity and creep

2.1.1. The Orowan mechanism: dislocation curvature vs obstacle spacing. Consider the interaction between a dislocation and an array of hard obstacles which are impenetrable for the dislocation (Fig. 3). The dislocation is forced to bow out between the obstacles—this is the primary effect responsible for all particle strengthening mechanisms. Plastic deformation due to long-range dislocation motion requires dislocations to fully bypass the obstacles (the “Orowan mechanism” [2]). The relevant size parameter for this case, given by the microstructure, is the obstacle spacing L. The bypass condition is reached when the characteristic length $d(\tau)$ approaches (or comes to lie below) L, i.e.

$$d(\tau) \leq L. \tag{2}$$

In other words, plastic deformation requires the dislocation loops (or half-loops) to fit between two neighboring obstacles [Fig. 3(b)]. This geometric requirement is expressed by the inequality [equation (2)], which sets into relation the two length scales, one (L) characteristic for the microstructure and the other (d) for the mechanism.

Combining equations (1) and (2) gives the bypassing stress or “Orowan stress” τ_{Or} in shear

$$\tau_{\mathrm{Or}} = \frac{2T_d}{bL} \approx \frac{Gb}{L} \propto \frac{Gb}{R} \tag{3}$$

where the proportionality establishes a connection

Fig. 3. The onset of plastic flow controlled by obstacles, seen as a size effect: plasticity requires bypassing of strong obstacles by dislocations, equivalent to the condition that a dislocation loop fit between neighboring obstacles. The size parameter is a (suitable average of the) obstacle spacing L, the characteristic dimension is the diameter $d(\tau)$ of a (fictitious) dislocation loop at a shear stress τ [equation (1)]. Case a: $d > L$, no deformation; case b: $d = L$, deformation. For penetrable obstacles these requirements are modified as described in the text.

with the radius R at constant volume fraction of particles.

Equation (3), which is at the heart of mechanical metallurgy, describes the maximum flow stress increase a dispersion of obstacles can impart in a dislocation-dominated material. It reflects a classical size effect: a finer dispersion results in more efficient hardening. In technical alloys, in which particle spacings and sizes are typically in the ranges 10–1000 and 1–100 nm, respectively, strength increases of several hundred MPa can be achieved in this way.

We note that the treatment given here covers only first-order effects. More sophisticated theories have long been available, which define an "average" value of L in arrays of statistically distributed obstacles, e.g. Refs [3, 4], or examine the effects of elastic anisotropy and of dipole interaction on line tension [5].

A special case of the treatment above is the phenomenon of *work hardening*. Here, the obstacles are forest dislocations and the relevant size parameter is given by their average spacing:

$$L = \frac{1}{\sqrt{\rho}} \tag{4}$$

where ρ is the dislocation density. Requiring again that $L = d$, we get the classical Taylor equation for work hardening:

$$\tau = \alpha G b \sqrt{\rho} \tag{5}$$

where $\alpha < 1$ accounts for the fact that dislocations are "penetrable" obstacles.

2.1.2. Effects of obstacle strength: age hardening. Many obstacles are not impenetrable to the dislocation, but "give" at a shear stress substantially below the Orowan stress. Such "weak" obstacles are, for example, solute atoms or coherent precipitates. In these cases, modifications of the concept have been found necessary.

First, the dislocation can now be released from the obstacles before the limiting condition given by equation (2) is met. A new condition can be formulated as follows:

$$d(\tau) \leq L\left(\frac{2T_d}{F_\mathrm{m}}\right) \tag{6}$$

where F_m is the maximum force sustained by the obstacle. The factor $(2T_d/F_\mathrm{m})$ describes the obstacle strength (for details see, e.g. Brown and Ham [6]). Note that in the case of impenetrable obstacles, for which $F_\mathrm{m} = 2T_d$, this and the following expressions reduce to those of Section 2.1.1.

Second, the obstacle spacing is now no longer a constant given by the microstructure, but depends also on the strength of the obstacle ("Friedel effect"). Weaker obstacles force the dislocation to bow out less, which, in a random particle array, causes the dislocation to encounter fewer obstacles along its length. This effect can be incorporated in the present approach by introducing a modified size parameter L^* which depends on F_m [6]:

$$L^* = L\left(\frac{2T_d}{F_\mathrm{m}}\right)^{1/2}. \tag{7}$$

Combining equations (1), (6) and (7) leads to a standard equation of the "cutting stress" for weak obstacles [6]:

$$\tau = \frac{Gb}{L}\left(\frac{F_\mathrm{m}}{2T_d}\right)^{3/2}. \tag{8}$$

Shearable particles, for which F_m scales with R, impart strengthening of the following form:

$$\tau \propto R^{1/2}. \tag{9}$$

It is important that the cutting stress scales with $\sqrt{R}$, in contrast to the bypassing stress [equation (3)] with a $1/R$-dependence.

These opposite size effects are the basis for *age-hardening* behavior of precipitation-strengthened systems. Figure 4 illustrates schematically a simple ageing curve constructed using equations (3) and (9). The maximum yield stress, corresponding to the "peak-aged" conditions, occurs at the transition from cutting to bowing, i.e. at a critical particle radius $\hat{R}$ which reflects the particle properties and is, at the present level of approximation, independent of volume fraction. This treatment, of course, neglects subtleties such as the loss of coherency with increasing particle size or the transformation sequence of metastable phases. Depending on the

Fig. 4. Age hardening in precipitation strengthened alloys: a classic size effect resulting from a $\sqrt{R}$-dependence of the cutting stress [equation (9)] and a $1/R$-dependence of the bypassing stress [equation (3)]. This causes a maximum in yield stress σ_y vs particle radius R at a characteristic value $\hat{R}$.

desired properties, a heat treatment may be chosen to give an optimum yield stress. This strategy, which is today an important technological concept, illustrates the main theme of this paper: the application of different size effects brought about by length scale interaction.

2.1.3. Creep strength and particle size. At high temperatures, lattice dislocations gain a new degree of freedom: they can now circumvent obstacles by climb or cross-slip, both of which are aided by thermally-activated processes. Successful high-temperature alloys therefore contain obstacles which are

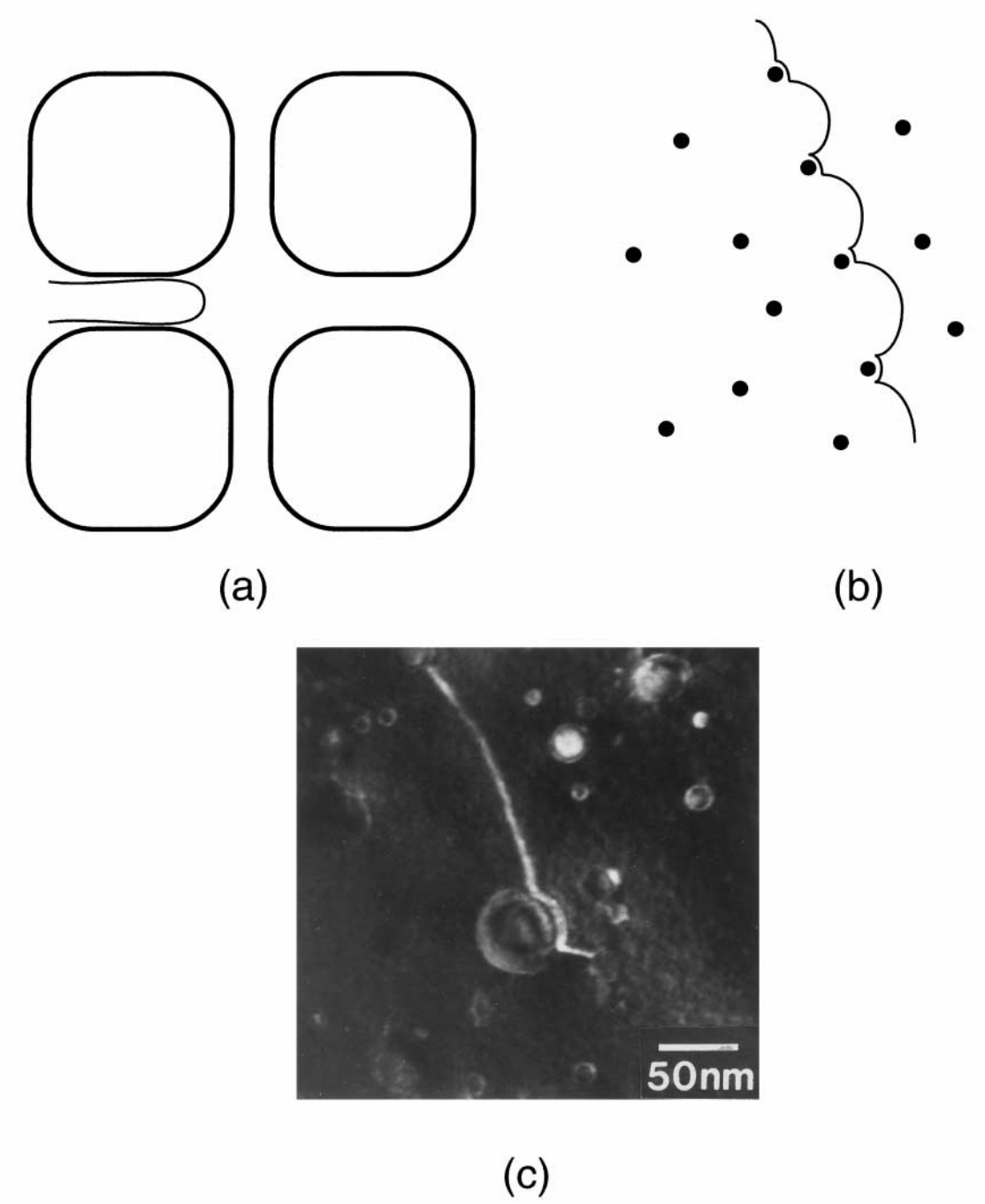

Fig. 5. Size effects in particle strengthening against creep: dislocations are forced to bend by (a) "channeling" through interparticle regions (as in superalloys), or by (b) attractive interactions with fine dispersoids (as in dispersion-strengthened alloys). A classic example of a TEM micrograph showing the attractive interaction is given in (c) (from Schröder and Arzt [7]).

not easily surmounted by these mechanisms (Fig. 5): (a) coarse precipitates which confine dislocation motion to the narrow channels between them (e.g. γ' particles in conventional Ni–base superalloys), or (b) fine dispersoids which pin the dislocations by exerting an attractive interaction on them (e.g. in dispersion-strengthened superalloys). In both instances pronounced size effects arise. In the first case the relevant size parameter is the width of the channels [8], which plays a similar role as the film thickness in thin-film plasticity (see Section 4.1 below); in the second case, the following particle size effect occurs.

The only way in which small obstacles can effectively impede the climb + glide motion of dislocations at high temperature is by exerting an attractive force on them [Fig. 5(c)]. This effect, which has repeatedly been observed by TEM, e.g. Refs [7, 9], can be attributed to the partial relaxation of the dislocation strain field by diffusion in the particle–matrix interface [10]. The attraction can be modeled by assigning a lower line energy ($\kappa \cdot U_{el}$ where $\kappa<1$) to the dislocation segment at the interface compared to the segment in the matrix (U_{el}) [11]. It has been shown that only a small relaxation is necessary for dislocation detachment from the particle to become the rate-determining event. By considering thermally-activated detachment, Rösler and Arzt have developed an equation for the creep strength of the following form [12]:

$$\frac{\tau}{\tau_d} = 1 - \frac{1}{1-\kappa}\left[\frac{kT \ln \dot{\varepsilon}_0/\dot{\varepsilon}}{Gb^2 R}\right]^{2/3} \tag{10a}$$

Fig. 6. Schematic of the creep strength (normalized) vs particle radius (normalized by the Burgers vector) for dispersion-strengthened materials [equation (10a)]. An optimum particle size (at a given volume fraction) arises because of the interplay between a high bypassing stress and thermally-activated detachment from small particles [12].

where T is the absolute temperature, k is Boltzmann's constant, $\dot{\varepsilon}$ the strain rate, $\dot{\varepsilon}_0$ a factor containing the diffusivity and the mobile dislocation density, and τ_d is the "athermal" detachment stress:

$$\tau_d = \tau_{Or}\sqrt{1-\kappa^2}. \tag{10b}$$

A normalized creep strength is plotted, for constant volume fraction, as a function of normalized particle radius in Fig. 6. It is seen that the creep strength improves at first with decreasing particle size; this is due to the increase in the Orowan stress, which enters in equation (10b). However, for even finer dispersoids, the probability of thermal detachment of dislocations is raised. The optimum particle size is predicted as

$$R_{opt} \approx \frac{kT}{Gb^2}\frac{2\ln(\dot{\varepsilon}_0/\dot{\varepsilon})}{(1-\kappa)^{3/2}}. \tag{11}$$

Depending on the strength of the particle–dislocation interaction (κ), this value typically lies in the nanometer range. Like in age hardening, arbitrarily fine dislocation obstacles are not desirable.

A more complicated case, which has only recently been considered, is dispersion strengthening of *ordered* matrix materials such as intermetallic alloys. There, the lattice dislocations frequently dissociates into partial (or "superpartial") dislocations which interact individually with the dispersoid [13] and, in addition, with each other (Fig. 7). The detachment process for such a case has been modeled, under certain simplifying assumptions, by Göhring and Arzt [14–17]. It is found that again the interaction of two length scales becomes decisive: the characteristic length is the spacing w of the superpartial dislocations, and the relevant size parameter is given by the particle diameter $2R$. Optimum creep strength is predicted for a characteristic ratio between the two ($w/2R \approx 0.6$). Indeed, evidence for such an effect, supported by extensive TEM observations [18], has recently been found in $Fe_{1-x}Al_x$ compounds with varying composition and hence superpartial spacing [15].

This case is an example for the interaction of two length scales which characterize a heterogeneity on different levels, i.e. that of the microstructural feature and that of the defect itself. A similar situation arises in magnetism, where the width of the domain walls interacts with the size of non-magnetic inclusions (see Section 3).

2.2. Grain size effects in plasticity and creep

2.2.1. Hall–Petch effect. Strengthening of polycrystalline materials by grain size refinement is technologically attractive because it generally does not adversely affect ductility and toughness. The classical effect of grain size on yield stress [19, 20] can, among other possibilities, be explained by a model invoking a pile-up of dislocations against grain boundaries, which results in a dependence of the

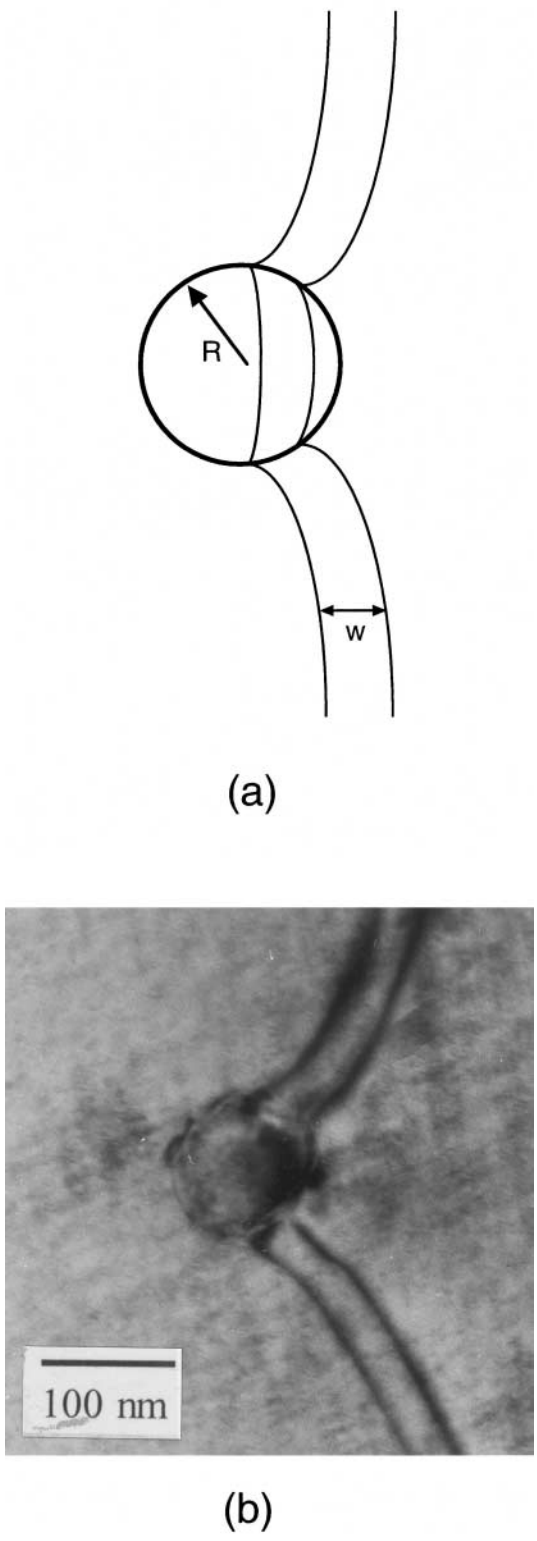

Fig. 7. Dislocation–particle interaction in ordered matrix materials: as dissociated superpartials interact individually with the particle (a), the characteristic length is the spacing w between the partials and the size parameter the particle radius R. The creep behavior is influenced by the ratio between the two. A TEM weak-beam micrograph of superdislocation–particle interaction in Fe–30 at.%Al is shown in (b) (after Behr *et al.* [13]).

hardening increment on the square root of the grain size D:

$$\tau = \frac{k_{\mathrm{HP}}}{\sqrt{D}} \tag{12}$$

where k_{HP} is a constant. This is the classical Hall–Petch effect.

2.2.2. Limits to Hall–Petch behavior: dislocation curvature vs grain size. Whereas many metallic materials obey such a relationship over several orders of magnitude in grain size (e.g. Ref. [21]), it is inevitable that the reasoning behind equation (12) must break down for very small grains. A clear limit for the occurrence of dislocation plasticity in a polycrystal is given by the condition that *at least one dislocation loop must fit into an average grain* [Figs 8(a) and (b)]. The characteristic length, i.e. the loop diameter [equation (1)], must now be compared with the grain size D as the relevant size parameter:

$$d(\tau) = D \tag{13a}$$

or

$$\tau = \frac{2T_d}{bD} \approx \frac{Gb}{D}. \tag{13b}$$

Figure 8(c) illustrates schematically this limit on Hall–Petch behavior: "conventional" grain size strengthening can be expected only to the right of the heavy line which signifies the limiting condition (13a)–(b). For Cu, as an example, the criticial grain size estimated in this way is about 50 nm; this value is in reasonable agreement with experimental results by Chokshi *et al.* [23], as shown in Fig. 9. Similar estimates have been made for different materials by Nieh and Wadsworth [24].

The plastic behavior of nanocrystalline materials with grain sizes below the critical value is not fully clear. Some authors (e.g. Refs [25–27]) also report an "inverse" Hall–Petch effect, others find an insensitivity to grain size or a reduced Hall–Petch constant k_{HP} in this range. It has been argued that because of the viscous behavior of amorphous materials (which can be considered the limiting case for grain refinement) the grain size strengthening effect will have to be reversed once the grain size D starts to approach the grain-boundary thickness δ_{b}. In fact, expectations of superplasticity in otherwise brittle ceramics rely on such an effect [28].

One possible explanation for such a softening effect comes from a re-consideration of the line tension T_d in equation (13b). The more refined expression

$$T_d = \frac{Gb^2}{4\pi} \ln \frac{r_1}{r_0} \tag{14}$$

contains a lower (r_0) and an upper (r_1) cut-off distance for the stress field of the dislocation. In conventional materials r_1 generally lies in the

Fig. 8. Grain size strengthening, as explained by pile-ups of dislocation loops against grain boundaries (a). This mechanism must break down when the diameter d of the smallest loop no longer fits into a grain of size D (b). The limiting condition is shown as the heavy line in (c) where the shear strength τ is plotted schematically as a function of grain size D. Hall–Petch behavior can only be found to the right of this line; abnormal or inverse behavior may result otherwise. The dotted line reflects schematically the Scattergood–Koch [22] equation [equation (16)].

micrometer range and therefore significantly exceeds r_0 (for which values between 2 and $10b$ are commonly assumed); this justifies replacing the logarithmic term by a constant. However, in nanocrystalline materials it is reasonable to equate r_1 to the grain size, which now gives $r_1 \approx r_0$ and makes T sensitive to the value of the grain size D. Therefore, we now have a case in which the characteristic length (d) is a function of the size parameter (D).

The resulting strength increment is given by

$$\tau = \frac{Gb}{2\pi D} \ln \frac{D}{r_0}. \tag{15}$$

This expression vanishes rapidly as the grain size D approaches the lower cut-off distance r_0. An even more refined expression has been obtained by Scattergood and Koch [22]. They draw upon Li's model [29] for the generation of dislocations from grain-boundary sources: as the dislocation density ρ

Fig. 9. Inverse Hall–Petch behavior in nanocrystalline Cu ($\bar{H} - \bar{H}_0$ denotes the hardness increment, D the grain size): the classical behavior breaks down at a grain size of about 50 nm, in agreement with an estimate based on the loop diameter [equations (13a)–(b)]. Replotted after Chokshi *et al.* [23].

scales inversely with grain size D, the obstacle spacing is $L \sim 1/\sqrt{\rho} \sim \sqrt{D}$, which yields

$$\tau \approx \frac{Gb}{\sqrt{D}} \ln \frac{D}{r_0}. \tag{16}$$

This expression, which is schematically shown as a dotted line in Fig. 8(c), reduces correctly to Hall–Petch behavior for $D \gg r_0$. It gives a possible interpretation of grain-boundary softening behavior in nanocrystalline Cu and Pd [22].

2.2.3. Diffusional creep as a size effect. An alternative explanation of grain-boundary softening in very fine-grained materials can be based on increasing contributions of diffusional creep. Diffusional processes in a potential gradient [caused in this case by a normal stress gradient, Fig. 10(a)] exhibit a natural size effect because the length scale affects the magnitude of the gradient. For maintaining a constant strain rate $\dot{\varepsilon}$ by diffusion of atoms from grain boundaries under compression to those under tension, the following shear stress τ is required [30, 31]:

$$\tau = \frac{\dot{\varepsilon} k T D^2}{C_1 D_v \Omega}. \tag{17}$$

Here D_v is the volume diffusivity, Ω the atomic volume, and C_1 a dimensionless constant of the order of 10. Accounting for grain-boundary diffusion (with diffusivity D_b through a grain boundary with thickness δ_b) gives [32]

$$\tau = \frac{\dot{\varepsilon} k T D^3}{C_2 \delta_b D_b \Omega}. \tag{18}$$

In addition to this, the triple lines in nanocrystalline materials can also act as fast diffusion paths [33]. Equations (17) and (18) reflect grain size effects which are opposite in direction and far stronger than those of dislocation plasticity (Hall–Petch effect). They are due to the increase, with finer grain size, in the volume fraction of "disordered"

Fig. 10. Diffusional creep is driven by gradients in normal tractions on grain boundaries (a). Fine arrows delineate the paths for transport of matter. This mechanism ceases to operate (b) once a grain boundary dislocation loop no longer fits into a grain facet ($d > D'$). Note the analogy with Fig. 8 for lattice dislocations.

material which can act as short-circuit diffusion path, and to the higher density of sinks and sources for matter.

It is still a matter of debate whether grain-boundary softening, which has occasionally been reported for nanocrystalline materials, can be attributed to these effects at room temperature. Chokshi *et al.* [23] claim that agreement of equation (18) with their results on Cu can be obtained by using a reduced value of the activation energy for grain-boundary diffusion (62 instead of 104 kJ/mol). Nieh and Wadsworth [24], by contrast, argue that such a comparison neglects the large differences in the grain size exponents (Fig. 9): according to equation (18), $\tau \sim D^3$ would be expected, whereas the observed behavior is closer to $\tau \sim D^n$ with $n<1$.

A new element is introduced in this discussion by noting that in very small grains the rate of creep may no longer be controlled by the diffusion step [as is tacitly assumed in equations (17) and (18)], but by the deposition and removal of atoms at the grain boundaries. Ashby [34] and Arzt *et al.* [35] have shown that for such "interface-controlled" diffusional creep the grain size dependence is much weaker:

$$\tau = \left(\frac{\dot{\varepsilon} k T G b_b}{C_4 \Omega D_{eff}} \right)^{1/2} D^{1/2}. \tag{19}$$

This result was obtained by modeling the interface reaction as the climb motion of an array of grain-boundary dislocations. Here D_{eff} is an effective diffusivity, b_b the Burgers vector of a boundary dislocation and C_4 another numerical constant. The $D^{1/2}$-proportionality, which results from the assumption of a stress-dependent dislocation density, is in better agreement with the data of Chokshi *et al.* (Fig. 9). However, because of the reduced grain size dependence, an even lower activation energy (about 40 kJ/mol) for diffusion has to be assumed to predict realistic deformation rates at room temperature.

Also, the motion of grain boundary dislocations is subject to a similar grain size limit as for lattice dislocations: models based on their presence must break down once an average grain facet of diameter D' can no longer accommodate a *grain-boundary* dislocation loop [Fig. 10(b)]. The corresponding limiting condition is, in analogy with equation (13b), given by

$$\tau = \frac{G b_b}{D'}. \tag{20}$$

The value of b_b corresponds to the difference in Burgers vector between two lattice dislocations and is therefore only a fraction of b. Hence, a stress window will exist in which plasticity due to lattice dislocations is suppressed or slowed down [at stresses below that given by equation (13b)], but diffusion creep operates because grain-boundary dislocations are still present and mobile.

Overall, the topic of plastic deformation and creep in nanocrystalline materials is by far not fully understood. The conditions for the appearance of abnormal Hall–Petch behavior, in particular, are not clear and controversial reports have been published. In addition, there is no accepted theoretical model, and the phenomenon is open to other interpretations.

3. THE ANALOGY WITH MAGNETIC STRENGTHENING

We now turn briefly to a different class of phenomena, which nevertheless displays interesting analogies to mechanical behavior, as suggested by Haasen [36, 37]. Ferromagnetism is due to spontaneous magnetization, i.e. the parallel alignment of electron spins along "easy" crystallographic directions. Because of the multiplicity of such directions in crystals of high symmetry a "magnetic microstructure" consisting of magnetic domains with uniform magnetization is formed; the domains are separated from one another by domain walls in which the spin direction rotates smoothly between the easy directions of the adjacent domains. The magnetization occurs, to a large extent, by the growth of domains oriented favorably with regard to the external magnetic field. This process requires the motion of the domain walls, whose interaction with defects determines the ease of magnetization (i.e. the coercive field).

The most fundamental length scale in magnetism is the domain wall thickness in the unperturbed lattice. It is, like the spacing of partial dislocations (Section 2.1.3), determined by two competing size effects: the quantum–mechanical exchange interaction, favoring parallel spins, tends to widen the wall; the crystal anisotropy, which maintains "easy" spin directions, encourages rapid spin rotation. The wall thickness is set by an energy minimum and is a material parameter:

$$\delta = \pi \left(\frac{A}{K_1} \right)^{1/2} \tag{21}$$

where A is the magnitude of the exchange integral and K_1 the magnetic anisotropy constant. The quantity δ is (except for the factor π) identical with the "exchange length", i.e. the minimum length over which the magnetization can vary appreciably. Values for δ range, e.g. from about 200 nm for Ni to about 3 nm for $Fe_{14}Nd_2B$. For magnetic phenomena, the wall thickness is an important characteristic dimension; its interaction with microstructural size parameters will now be addressed.

3.1. Particle strengthening in magnetism

The interaction of domain walls with magnetic inhomogeneities is analogous to dislocations [36, 37]

or grain boundaries [38] interacting with a field of particles. Consider a microstructure with non-magnetic particles of radius R in a ferromagnetic matrix. A major contribution to the "hardness" of such a magnet, characterized by its coercive field H_c, comes from the reduction in wall energy, which has to be supplied by the magnetization energy as the wall pulls away from the particles.

For geometric reasons, two limiting cases are generally distinguished: for a particle which is much smaller than the wall thickness ($R \ll \delta$), the maximum force exerted on the wall is

$$F_m \approx \frac{R^3\gamma}{\delta^2} \tag{22}$$

where γ is the domain wall energy per unit area. The resulting coercive field is then, in the simplest case, given by

$$H_c \propto \frac{\gamma R}{\delta^2}. \tag{23}$$

The magnetic "strength" is therefore expected to increase with particle size in this limit.

Large particles ($R \gg \delta$) exert a maximum force of

$$F_m \approx 2R\pi\gamma \tag{24}$$

which gives an inverse relationship between H_c and R:

$$H_c \propto \frac{\gamma}{R}. \tag{25}$$

Because of the different particle size dependencies, a maximum in magnetic strength is expected when

$$R \approx \delta. \tag{26}$$

Thus, a direct analogy with age hardening, as discussed in Section 2.1.2, becomes apparent. It is emphasized that our simple derivation neglects important effects of particle statistics, whose incorporation can give modified R-dependences [36, 39]. Also, detailed experimental verification of equation (25) is difficult, because other effects, such as stray fields or magnetostrictive interactions with coherency stresses of the particles, may superimpose on the mechanism considered here (e.g. Ref. [39]). This principle of magnetic age hardening has been exploited in the development of mechanically strong, but magnetically soft alloys. In this case the mechanically "peak-aged" condition corresponds to fine particle sizes which are "under-aged" with respect to magnetic properties—a technical application of size effects in different property domains.

3.2. Grain size effects in magnetism

In polycrystalline ferromagnets, grain boundaries are, by necessity, magnetic domain boundaries (whereas the converse is of course not true). As the domain wall mobility is determined by the volume density of these defects, the coercive field increases with decreasing grain size in the following way [38, 40]:

$$H_c = H_{c,o} + \frac{k_M}{D} \tag{27}$$

where $H_{c,o}$ reflects the coercivity due to other effects, such as internal stresses, impurities, inclusions, etc. The constant k_M contains the wall energy and other magnetic properties of the material.

Thus, when the grain size is progressively refined, the magnetic "hardness" increases (Fig. 11). However, because of the interaction beween domain walls and grain boundaries, we expect this dependence to break down for

$$\delta \approx D. \tag{28}$$

Indeed, the grain size dependence reverses at a value close to the wall thickness (Fig. 11). The value of H_c then decreases rapidly to values comparable with those for amorphous soft magnets. Such a behavior can be seen as an analogy to the dependence of the yield stress on grain size (cf. Fig. 9).

The reason for the strong drop in coercivity at grain sizes below the wall thickness lies in a new micromagnetic mechanism: the ferromagnetic exchange interaction, which now extends over several grains, tends to align the magnetic moments, overriding the "easy" directions of each individual grain. As a result, the anisotropy is reduced and, following equation (21), the domain wall thickness is further increased. This effect leads to a strong grain-size dependence of the coercive field [41–43]:

$$H_c \propto D^6. \tag{29}$$

Nanocrystalline magnets have been developed in the last decade which exhibit exceptional soft-magnetic properties [41, 44]. The system Fe–Cu–Nb–Si–B has been found to be particularly promising because, in addition to the reduced anisotropy, also the magnetostriction practically vanishes in the nanocrystalline state. Compared to conventional soft magnets, this new material class offers decisive advantages in magnetic properties (e.g. a substantially improved saturation polarization).

4. MECHANICAL STRENGTH OF THIN FILMS: THE DIMENSIONAL CONSTRAINT

Thin films are by definition materials in which one dimension (that in the "thickness" direction) is much smaller than the other two. It can then be expected that the size constraint, rather than the microstructure, will control the mechanical properties. Also transport properties have been found to exhibit size effects: the electrical and thermal conductivity of thin films, for example, decrease significantly once the film thickness is reduced below the mean free path of electrons or phonons.

Fig. 11. Grain size effects in magnetism (after Herzer [41]): The coercive field follows classically a $1/D$ (where D is the grain size) dependence. For very small grains, a D^6 proportionality is found. The maximum magnetic "hardness" occurs when the grain size D is comparable to the width δ of a domain wall. Note the analogy with mechanical strengthening (Fig. 9).

The obvious size parameter for a thin film is its thickness H. An important complication in polycrystalline thin films is the fact that this size constraint often causes a microstructural constraint: normal grain growth usually stagnates once the grain size is comparable to the film thickness [45]. As a consequence, thin films generally consist of relatively fine grains, unless they are deposited epitaxially on single crystal substrates or heat treated in a way to encourage abnormal grain growth [46]. The grains often extend through the thickness of the film ("columnar grains") such that the film can be thought of as a two-dimensional array of single crystals.

An important property of thin films which has been studied extensively in recent years is their plastic yield stress. This property is of practical importance because it can affect the reliability of thin-film components. In terms of micromechanisms, thin-film plasticity is influenced by the dimensional constraint on dislocation motion, which results in a pronounced size effect.

4.1. Film thickness and yield stress: the "dislocation channeling" mechanism

Consider a single-crystalline film attached to a substrate and subjected to a biaxial stress in the film plane. We wish to determine the shear stress τ_y necessary to cause yielding by the motion of dislocations, which are constrained to "channel" through the film. A first estimate is obtained by requiring a dislocation loop to fit inside the film (Fig. 12); if the film surface is impenetrable to the dislocation (e.g. because of the presence of an oxide layer), the limiting condition becomes, in analogy with equation (2) [Fig. 12(a)]

$$d(\tau) = H' \tag{30}$$

or, equivalently

$$\tau_y = \frac{G_f b}{H'} \tag{31}$$

where $d(\tau)$ is again the characteristic loop diameter [equation (1)], G_f the shear modulus of the film and

Fig. 12. The dimensional constraint on plasticity in thin films: the yield stress can be estimated by requiring a "dislocation loop" to fit into the film ($d<H'$). H' depends on the film thickness H and the orientation of the slip plane (see Fig. 2). Case a: impenetrable film surface; case b: "free" film surface.

$H' = H/\sin\varphi$ the size parameter (where φ is the angle between the normal to the plane of the loop and the film normal). This expression is similar to the Orowan stress [equation (3)], with the obstacle spacing L replaced by H'.

Alternatively, if the film surface is "free" and exerts attractive image forces on the dislocation, it is sufficient to fit half a loop into the film [Fig. 12(b)]. The stress estimate is then half of that given in equation (31). It is, however, generally found (e.g. Ref. [47]) that equation (31), which has been suggested in similar form early in the development of thin-film mechanics [48], substantially underestimates the yield stress.

A more sophisticated model has been developed by Freund [49] and Nix [47]. As a dislocation advances in a film by "channeling", it creates additional line length in the interfaces. The energy of these "misfit dislocations" is, in the presence of an elastically stiffer substrate and, possibly, an oxide layer, raised against the line energy far from the interface. An energy balance between the work done by the dislocation and the energy stored in the misfit dislocation arms leads to a result in which G_f [in equation (31)] must be replaced by an "effective" shear modulus given by

$$G_{\text{eff}} = \frac{G_f}{2\pi(1-\nu)}\left[\frac{G_s}{G_f+G_s}\ln\frac{\beta_1 H}{b} + \frac{G_o}{G_f+G_o}\ln\frac{\beta_2 H_o}{b}\right]. \quad (32)$$

Here the subscripts s and o refer to substrate and oxide layer, respectively, H_o is the thickness of the oxide layer, β_1 and β_2 are constants defining the cut-off radii, and ν is Poisson's number of the film. The "free"-surface case is readily obtained by deleting the second term in equation (32). For stiff substrates, G_{eff} can exceed G_f considerably; therefore this modification predicts, in comparison with equation (31), much higher yield stresses. For coarse-grained Al films, the calculated values have been shown to agree well with experimental results, e.g. those of Venkatraman and Bravman [50]. They are about an order of magnitude higher than for bulk Al of the same purity—an impressive manifestation of the size constraint on dislocation motion.

Fig. 13. Separation of dimensional and microstructural constraints on plastic deformation of thin Cu films: the measured yield stresses σ_y scale with the reciprocal of film thickness H, but substantially exceed the prediction of equations (32) and (33) ("Nix–Freund model" [47, 49]). The discrepancy can be tentatively explained by a superposition of the thin-film effect with grain size (Hall–Petch) and with Taylor hardening (after Keller *et al.* [52]).

4.2. Grain size effects: Hall–Petch strengthening in thin films?

The remaining discrepancies between theory and experiments on polycrystalline films can be attributed to the interaction of the dislocation with grain boundaries. Following the simple treatment by Thompson [51], a grain-size dependent term can be included in the energy balance, which should give an additional contribution to the yield stress:

$$\tau_y^{gb} \approx \frac{G_f b}{D} \frac{\sin \varphi}{4\pi(1-\nu)} \ln \frac{\beta_3 D}{b}. \tag{33}$$

As a consequence, grain size strengthening in thin films would not be expected to exhibit Hall–Petch behavior. There is in fact circumstantial evidence for this conclusion [50].

A recent study on the yield stress of polycrystalline copper films, however, leads to a different result. Keller *et al*. [52] found that the thin-film contribution [equations (31) and (32)] explained only a fraction of the stresses measured (Fig. 13). It should be noted that, after normalizing with G_{eff}, stress values for both unpassivated and passivated films fell on the same straight line; the effect of the passivation therefore seemed to be correctly accounted for by the Freund–Nix model. The data could best be fitted by superimposing on the film thickness effect a grain-boundary contribution following a Hall–Petch relation [equation (12)], but with a constant k_{HP} three times the value commonly found for bulk materials. Alternatively, the experimental stresses could also be explained by a superposition of thin-film effect, Hall–Petch effect and a contribution from dislocations (Taylor hardening). Besides this uncertainty, it is not fully clear at present whether the Hall–Petch or the Thompson description is more generally valid for thin films. The issue of grain size strengthening in thin films, and in particular the superposition of dimensional and microstructural constraints, will therefore require further studies in the future.

4.3. Hardness of multilayers: "channeling" vs interface penetration of dislocations

As a final example, we consider epitaxial multilayers, which consist of alternating layers of two dissimilar materials. Such thin-film "superlattices" exhibit interesting electrical, optical, and magnetic properties and are attractive for many technological applications ranging from X-ray mirrors to hard disk media and magnetoresistive sensors. Their mechanical properties are also remarkable: for example, the hardness values, as measured by nanoindentation through many consecutive layers, are considerably enhanced over those measured for the pure films of the two components (Fig. 14 [53]). This property shows a clear size effect with respect to the bilayer period Λ, i.e. the sum of the two individual layer thicknesses. On decreasing Λ, the hardness rises at first, reaches a plateau and then decreases sharply.

Daniels [53] argues that the hardness maximum is due to two competing effects: at large bilayer periods, dislocation pile-ups are assumed to favor the penetration of dislocations from one layer into the adjacent layer. The resulting Hall–Petch description is in good agreement with the data (Fig. 14); an explanation based on dislocation channeling, however, has also been found to be a viable alternative. At small Λ, dislocation penetration is no longer aided by pile-ups, but is instead controlled by image stresses due to the discontinuities in elastic modulus. Following earlier models [54–58], the analysis by Daniels leads to a prediction which is in good agreement with the experiment for

Fig. 14. Size effect in a multilayer thin-film system [53]: the hardness of an epitaxial sputter-deposited Fe(001)/Pt(001) multilayer exhibits, as a function of bilayer period Λ at equal layer thicknesses, a maximum. The lines show the results of a model by Daniels [53]: penetration of a dislocation through the multilayer interfaces is controlled by pile-ups (Hall–Petch effect) at large Λ, and by image stresses at small Λ. Note that all hardness values considerably exceed those of the pure materials (Fe: 4.8 GPa, Pt: 2 GPa) or of a rule-of-mixtures calculation (3.4 GPa).

$\Lambda < 150$ nm (Fig. 14). The reverse size effect is attributed to the reduced image stresses acting in the forward direction as the bilayer thickness is increased. This model, which could be further refined to include "diffuse" interfaces or multiple dislocations [53], has proven to be successful in the description of the size effect on hardness in some multilayer systems.

Overall, the data in Fig. 14 are another convincing example of size effects in thin-film systems. As must be expected, the increase in strength with further miniaturization does not continue indefinitely but is subject to the intervention of alternative mechanisms with a different size dependence. We note that the maximum displayed in Fig. 14 is reminiscent of the breakdown of Hall–Petch behavior in nanocrystalline bulk materials (Fig. 9).

5. CONCLUDING REMARKS

Size effects are abundant in the materials world. In the present paper we have focussed on properties which are governed by the motion of defects such as dislocations, vacancies and domain walls. For such processes, size effects come about because an intrinsic property of the defect (its curvature, or its extension) interacts with a microstructural or a dimensional constraint. Other examples (not treated here) are the interaction of grain boundaries with particles, resulting in a characteristic equilibrium grain size ("Zener effect"), or the pinning of flux lines by inclusions in type II superconductors [37].

A question of considerable technological importance concerns the dimensional effects in micromachined components. It is obvious that the elastic behavior, for which the length of an atomic bond is the characteristic length, should not be affected by the microdimensionality. By contrast, dislocation plasticity, as has been discussed for thin films, is subject to strong size effects because of the much larger characteristic lengths involved; appreciable effects will appear for metallic components with sizes below several micrometers. It can further be expected that the local accumulation of plastic strain, such as in fatigue loading, will be affected at even larger component sizes: the self-organization of dislocation structures results in cells and slip bands which can extend over several tens of micrometers. The constraints on these processes may explain experimental evidence for increased fatigue life in thin metallic wires [59, 60]. Finally, the fracture behavior will also exhibit size dependencies: in ductile fracture a new mechanism must occur as the component dimensions fall below the size of fracture dimples observed in bulk materials. Also the fracture probability of brittle materials is known to decrease for smaller sizes, reflecting defect statistics; it is this effect which has contributed to the success of silicon as a mechanical material [61] for microsystems which, in large dimensions, could not be built reliably from such an intrinsically brittle material.

In retrospect, it is seen that size effects have unexpected commonalities in several otherwise unrelated phenomena: almost all properties addressed in this paper exhibit a maximum at a characteristic value of the size parameter: particularly clear examples are the yield stress as a function of particle size and of the bilayer period in multilayers, as well as the magnetic properties dependence on grain size. Other maxima are less well established, let alone understood, e.g. the yield stress of extremely fine-grained materials (breakdown of Hall–Petch behavior).

Formally, another commonality is visible in several size effects: they are the result of a balance between two quantities with different dependences on length. In the Orowan effect, the work done by a dislocation advancing between two particles scales with the obstacle spacing (or radius), whereas the balancing forces at the particles do not; similarly, in thin-film plasticity the elastic strain energy of the film scales with its thickness, whereas the energy of the interface dislocations left behind does not (or only weakly through a logarithmic dependence). In such cases the size effect can be traced back to a surface-to-volume ratio as the governing parameter. Other fields, such as biology, cannot escape such size effects either: because of surface-to-volume effects on metabolism, the average lifetime of mammals depends clearly on their size [62]. Biological evolution, too, is therefore subject to dimensional constraints and has found optimum sizes: trees are known not to grow into the skies.

Acknowledgements—This paper is based on the R. S. Williams Lectures 1996 given by the author in the Department of Materials Science and Engineering at the Massachusetts Institute of Technology. The author is grateful for this appointment. He would like to thank H. Fischmeister and W. D. Nix for a critical reading of the manuscript. The help of Jeff Mason in designing the figures is gratefully acknowledged.

REFERENCES

1. Underwood, E. E., *Quantitative Stereology*. Addison Wesley, Reading, Massachusetts, 1970.
2. Orowan, E., *Symposium on Internal Stresses*. Institute of Metals, London, 1947, p. 451.
3. Kocks, U. F., *Can. J. Phys*., 1967, **45**, 737.
4. Labusch, R., *J. appl. Phys*., 1977, **48**, 4550.
5. Ashby, M. F., *Acta metall*., 1966, **14**, 679.
6. Brown, L. M. and Ham, R. K., in *Strengthening Methods in Crystals*, ed. A. Kelly and R. B. Nicholson. Elsevier, Amsterdam, 1971, p. 9.
7. Schröder, J. and Arzt, E., *Scripta metall*., 1985, **19**, 1129.
8. Pollock, T. M. and Argon, A. S., *Acta mater*., 1992, **40**, 1.
9. Nardone, V. C. and Tien, J. K., *Scripta metall*., 1983, **17**, 467.
10. Srolovitz, D. J., Luton, M. J., Petkovic-Luton, R., Barnett, D. M. and Nix, W. D., *Acta metall*., 1984, **32**, 1079.

11. Arzt, E. and Wilkinson, D. S., *Acta metall.*, 1986, **34**, 1893.
12. Rösler, J. and Arzt, E., *Acta metall.*, 1990, **38**, 671.
13. Behr, R., Mayer, J. and Arzt, E., *Scripta mater.*, 1997, **36**, 341.
14. Arzt, E. and Göhring, E., *Scripta metall.*, 1993, **28**, 843.
15. Arzt, E., Behr, R., Göhring, E., Grahle, P. and Mason, R. P., *Mater. Sci. Engng*, 1997, **A234-236**, 22.
16. Göhring, E., Ph.D. dissertation, Universität Stuttgart, 1997.
17. Arzt, E. and Göhring, *Acta mater*, in press.
18. Behr, R., Mayer, J. and Arzt, E., *Intermetallics*, in press.
19. Hall, E. O., *Proc. R. Soc. Lond.*, 1951, **B64**, 474.
20. Petch, N. J., *J. Iron Steel Inst.*, 1953, **174**, 25.
21. Meyers, M. A. and Chawla, K. K., *Mechanical Metallurgy*. Prentice-Hall, Englewood Cliffs, New Jersey, 1984, p. 494.
22. Scattergood, R. O. and Koch, C. C., *Scripta metall.*, 1992, **27**, 1195.
23. Chokshi, A. H., Rosen, A., Karch, J. and Gleiter, H., *Scripta metall.*, 1989, **23**, 1679.
24. Nieh, T. G. and Wadsworth, J., *Scripta metall.*, 1991, **25**, 955.
25. Weertman, J. R., *Mater. Sci. Engng*, 1993, **A166**, 161.
26. Fougere, G. E., Weertman, J. R. and Siegel, R. W., *Nanostruct. Mater.*, 1993, **3**, 379.
27. Volpp, T., Göhring, E., Kuschke, W.-M. and Arzt, E., *Nanostruct. Mater.*, 1998, **7,** 855.
28. Karch, J., Birringer, R. and Gleiter, H., *Nature*, 1987, **330**, 556.
29. Li, J. C. M., *Trans. Am. Inst. Min. Engrs*, 1963, **227**, 239.
30. Nabarro, F. R. N., *Bristol Conf. on Strength of Solids*, 1948, p. 75.
31. Herring, C., *J. appl. Phys.*, 1950, **21**, 437.
32. Coble, R. L., *J. appl. Phys.*, 1963, **34**, 1679.
33. Wang, N., Wang, Z., Aust, K. T. and Erb, V., *Acta mater.*, 1995, **43**, 519.
34. Ashby, M. F., *Scripta metall.*, 1969, **3**, 837.
35. Arzt, E., Ashby, M. F. and Verall, R. A., *Acta metall.*, 1983, **31**, 1977.
36. Haasen, P., *Mater. Sci. Engng*, 1972, **9**, 191.
37. Haasen, P., *Contemp. Phys.*, 1977, **18**, 373.
38. Kersten, M., *Z. Phys.*, 1943, **44**, 63.
39. Träuble, H., in *Moderne Probleme der Metallphysik*, Vol. II, ed. A. Seeger. Springer, Berlin, 1966, p. 157.
40. Adler, E. and Pfeiffer, H., *I.E.E.E. Trans. Magn.*, 1974, **10**, 172.
41. Herzer, G., *Physica Scripta*, 1993, **T49**, 307.
42. Alben, R., Becker, J. J. and Chi, M. C., *J. appl. Phys.*, 1978, **49**(3), 1653.
43. Herzer, G., *I.E.E.E. Trans. Magn.*, 1990, **26**, 1397.
44. Yoshizawa, Y., Oguma, S. and Yamauchi, K., *J. appl. Phys.*, 1988, **64**(10), 6044.
45. Mullins, W. W., *Acta metall.*, 1958, **6**, 414.
46. Thompson, C. V., *A. Rev. Mater. Sci.*, 1990, **20**, 245.
47. Nix, W. D., *Metall. Trans.*, 1989, **20A**, 2217.
48. Murakami, M., Kuan, T.-S. and Blech, I. A., *Treatise on Materials Science and Technology*, Vol. 24. Academic Press, New York, 1982, p. 164.
49. Freund, L. B., *J. appl. Mech.*, 1987, **54**, 553.
50. Venkatraman, R. and Bravman, J. C., *J. Mater. Res.*, 1992, **7**, 2040.
51. Thompson, C. V., *J. Mater. Res.*, 1993, **8**, 237.
52. Keller, R.-M., Baker, S. P. and Arzt, E., *J. Mater. Res.*, 1998, **13,** 1307.
53. Daniels, B. J., Ph.D. thesis, Stanford University, Department of Materials Science and Engineering, 1995.
54. Koehler, J. S., *Phys. Rev. B*, 1970, **2**, 547.
55. Lehoczky, S. L., *J. appl. Phys.*, 1978, **49**, 5479.
56. Doerner, M. F., Ph.D. thesis, Stanford University, Department of Materials Science and Engineering, 1987.
57. Shinn, M., Hultman, L. and Barnett, S. A., *J. Mater. Res.*, 1992, **7**, 901.
58. Övecoglu, M. L., Doerner, M. F. and Nix, W. D., *Acta metall.*, 1987, **35**, 2947.
59. Hofbeck, R., Hausmann, K., Ilschner, B. and Künzi, H. U., *Scripta metall.*, 1986, **20**, 1601.
60. Judelewicz, M., Künzi, H. U., Merk, N. and Ilschner, B., *Mater. Sci. Engng*, 1994, **A186**, 135.
61. Petersen, K. E., *Proc. IEEE*, 1982, **70**, 420.
62. Lin, H., *Am. J. Phys.*, 1982, **50**(1), 72.

APPENDIX A

Nomenclature

Characteristic lengths

δ_b	grain-boundary thickness
δ	thickness of magnetic domain walls
d	diameter of a dislocation loop
w	pacing of superpartial dislocations.

Size parameters

D	grain size
H	film thickness
L	obstacle spacing
L^*	obstacle spacing for penetrable particles
R	obstacle radius
Λ	bilayer period of a multilayer.

Other symbols

A	ferromagnetic exchange integral
b	Burgers vector of a lattice dislocation
b_b	Burgers vector of a grain-boundary dislocation
γ	specific domain wall energy
D_v	lattice diffusivity
D_b	grain-boundary diffusivity
$\dot{\varepsilon}$	strain rate
F_m	maximum force
G	shear modulus
H_c	coercive field
$\bar{H}$	hardness
κ	relaxation factor
k	Boltzmann's constant
k_{HP}	Hall–Petch constant
K_1	magnetic anisotropy constant
Ω	atomic volume
ρ	dislocation density
T	absolute temperature
T_d	line tension
τ	shear stress
τ_d	detachment shear stress
τ_{Or}	Orowan stress in shear
U_{el}	line energy.